LITERATURE CITED

1. A. F. Ginevskii and A. S. Dmitriev, Coll. from Moscow Power Institute [in Russian], No. 149 (1987), pp. 5-24.
2. M. Dixon, AIAA Pap. No. 77 (1985), pp. 1-12.
3. E. M. Lifshits and L. P. Pitaevskii, Physical Kinetics [in Russian], Moscow (1979).
4. P. L. Kirillov, Yu. S. Yur'ev, and V. P. Bobkov, Handbook on Thermohydraulic Calculations: Nuclear Reactors, Heat Exchangers, and Steam Generators [in Russian], Moscow (1984).
5. O. Knake and I. N. Stranskii, Usp. Fiz. Nauk, No. 2, 261-305 (1959).
6. A. S. Davydov, Solid-State Theory [in Russian], Moscow (1976).
7. A. P. Prudnikov, Yu. A. Brychkov, and O. I. Marichev, Integrals, Series, and Elementary Functions [in Russian], Moscow (1981).
8. E. P. Muntz and M. Dixon, AIAA Pap. No. 305 (1985), pp. 1-15.

THE BOUNDARY LAYER ON A REGULAR DROPLET CHAIN IN CONTROLLED MOTION

V. I. Bezrukov, A. S. Vasil'ev,
N. A. Razumovskii, and E. F. Sukhodolov

UDC 532.5:66.069.83

The retardation of a droplet chain by air resistance has been examined. Lee's method gives nomograms for the boundary-layer thickness, velocity distribution near the chain, and chain retardation. Experiments show that the model is applicable to important cases.

Regular droplet chains may be used in directing the droplets to one, two, or three traps as well as in recording analog, graphic, and half-tone data and in printing parts of characters.

The viscous friction in air results in momentum transfer from the environment and boundary layers, while the chain itself is retarded. The boundary layer affects the following: the distances between nozzles in multijet printing; the sizes and positions of the traps and of the charging and deflecting electrodes; the lower edges to the characters; the correcting signals, etc. All droplets, no matter what their paths, travel various initial distances in the boundary layers. Figure 1 shows a physical model for determining the main boundary-layer features. Lee's method [1] has been modified for these conditions and gives a mathematical model for the boundary layer. We write the momentum conservation for the mass flows through the current cross section and through the end of the nozzle in the one-dimensional jet representation:

$$\rho_g 2\pi \int_0^{\delta(z)} [a(z)+y]\, v_g^2(z,\ y)\, dy + \rho_\ell \pi a^2(z)\, v_\ell^2(z) = \rho_\ell \pi a_0^2 v_\ell^2. \tag{1}$$

The rate of momentum loss along the path due to boundary-layer friction is

$$-\frac{d}{dz}\left[\rho_\ell \pi a^2(z)\, v_\ell^2(z)\right] = 2\pi a(z)\, \nu_g \left.\frac{\partial v_g(z,\ y)}{\partial y}\right|_{y=0}. \tag{2}$$

The condition for jet continuity is

$$\pi a^2(z)\, v_\ell(z) = \pi a_0^2 v_{\ell 0}. \tag{3}$$

The velocity profile for the air flow in the boundary layer in logarithmic approximation is

Electrojet Technology Center, Leningrad Fine Mechanics and Optics Institute. Translated from Inzhenerno-fizicheskii Zhurnal, Vol. 60, No. 4, pp. 661-668, April, 1991. Original article submitted October 24, 1990.

0022-0841/91/6004-0505$12.50

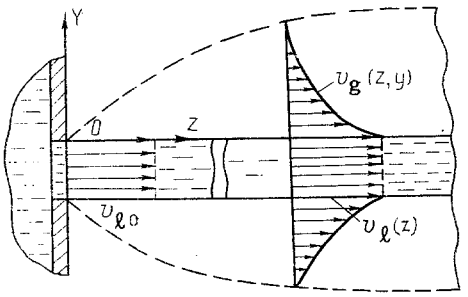

Fig. 1. Model for boundary-layer formation.

$$v_g(z,\ y) = v_\ell(z)\left[1 - \frac{1}{\beta(z)}\ln\left(1 + \frac{y}{a(z)}\right)\right], \tag{4}$$

in which

$$\beta(z) = \ln\left[1 + \frac{\delta(z)}{a(z)}\right] \quad \text{or} \quad \frac{\delta(z)}{a(z)} = e^{\beta(z)} - 1. \tag{5}$$

The boundary conditions in the boundary layer are

$$v_g(z,\ 0) = v_\ell(z), \tag{6}$$

$$v_g(z,\ \delta) = 0, \tag{7}$$

$$\left[\frac{\partial^2 v_g}{\partial y^2} - \frac{1}{a(z)}\frac{\partial v_g}{\partial y}\right]_{y=0}. \tag{8}$$

We transform this system, with a(z) replaced by expressions derived from (3):

$$\bar{v}_\ell(z) = \frac{v_\ell(\bar{z})}{v_{\ell 0}} = \frac{1}{1 - \bar{\rho}\left[1 + \frac{1}{\beta} - \frac{1}{2\beta^2}(e^{2\beta} - 1)\right]}, \tag{9}$$

$$\frac{d\bar{v}_\ell}{d\bar{z}} = -\rho\frac{\bar{v}_\ell(\bar{z})}{\beta(\bar{z})}. \tag{10}$$

Joint solution to the latter two equations gives

$$\frac{d\beta(\bar{z})}{d\bar{z}} = \frac{\beta^2 - \rho\left[\beta^2 + \beta - \frac{1}{2}(e^{2\beta} - 1)\right]}{\beta(1 + e^{2\beta}) - e^{2\beta} - 1} \tag{11}$$

or

$$\bar{z} = \int_0^\beta \frac{\beta(1 + e^{2\beta}) - e^{2\beta} - 1}{\beta^2 - \bar{\rho}\left[\beta^2 + \beta - \frac{1}{2}(e^{2\beta} - 1)\right]}\, d\beta, \tag{12}$$

in which

$$\bar{z} = \frac{4}{\mathrm{Re}}\frac{z}{a_0},\quad \mathrm{Re} = \frac{2a_0\rho_g v_{\ell 0}}{\mu},\quad \bar{\rho} = \frac{\rho_g}{\rho_\ell}. \tag{13}$$

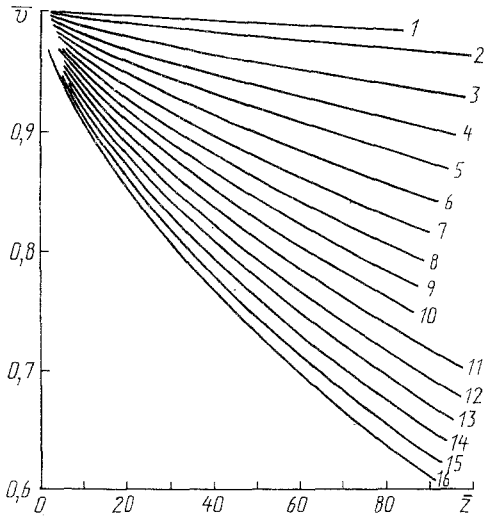

Fig. 2. Computer calculations on the change in jet speed with distance from nozzle for various $\bar{\rho}$: 1) 0.0005; 2) 0.001; 3) 0.002; 4) 0.003; 5) 0.004; 6) 0.005; 7) 0.006; 8) 0.007; 9) 0.008; 10) 0.009; 11) 0.01; 12) 0.011; 13) 0.012; 14) 0.013; 15) 0.014; 16) 0.015.

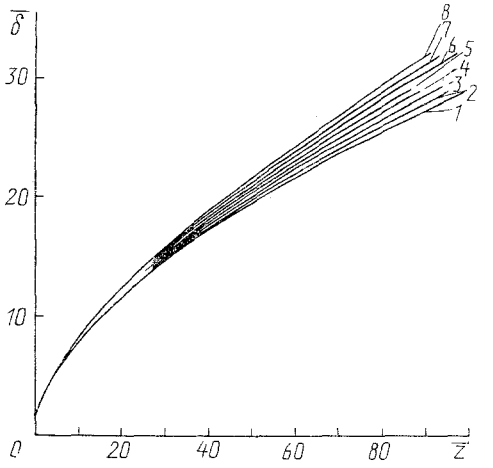

Fig. 3. Variation in boundary-layer thickness along jet for various $\bar{\rho}$: 1) 0.001; 2) 0.003; 3) 0.005; 4) 0.007; 5) 0.009; 6) 0.011; 7) 0.013; 8) 0.015.

This model has been used as follows.

With a given $\bar{\rho}$, (11) and (12) are integrated numerically to derive β as a function of $\bar{z}$ or vice versa, and then one calculates $v_{\ell}(z)$, $a(z)$, $\delta(z)$ and the velocity profile for the air jet $v_g(z, y)$. As there is a singularity (at $z = 0$, $\bar{\rho} = 0$, $\delta = 0$), the initial conditions are taken at a point remote from the end of the nozzle. Figures 2-4 show dimensionless computer results obtained on varying $\bar{\rho}$ over essentially the entire practical range. These families cover various liquids ranging from ink to molten metals and also short and long paths.

To use the results for a regular chain, it is sufficient to transform $\bar{\rho}$ and represent it for a droplet jet in air in terms of the effective density

$$\bar{\rho} = \frac{\rho_g}{\rho_\ell}\left(\frac{d_d}{d_n}\right)^2. \qquad (14)$$

Here $\bar{\rho}$ varies somewhat along the path. Figure 5 shows observed and numerical results for realistic cases $(d_n, v_{\ell 0}, \bar{\rho}, d_d, f_d, \lambda_d)$, where for air we took $\eta_g = 1{,}79 \cdot 10^{-2}$ mPa·sec, $\rho_g = 1.21$ kg/m^3, and $\nu_g = 1.49 \times 10^{-5}$ m^2/sec (at 20°C and 760 mm Hg). The algorithm based on this method includes the following operations:

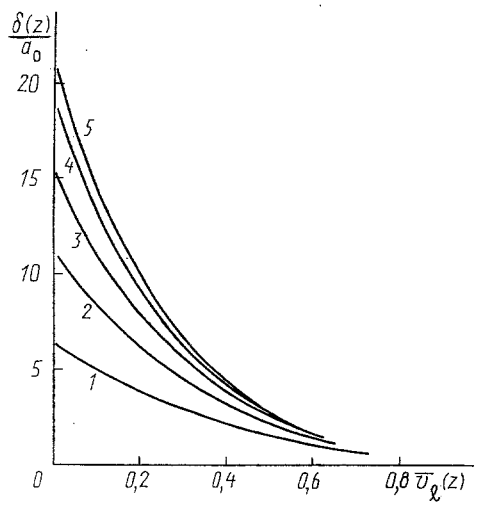

Fig. 4. Numerical simulation results for boundary-layer velocity profile along jet ($\bar{\rho}$ = 0.008): 1) $\bar{z}$ = 7; 2) 18.3; 3) 31.7; 4) 45.3; 5) $\bar{z}$ = 54.

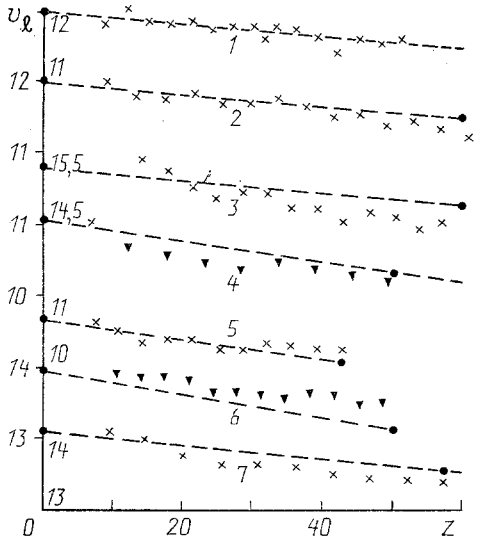

Fig. 5. Retardation of a regular droplet chain (trapped) along path for seven experiments: 1) d_n = 100 μm; f_d = 20 kHz, p = 150 kPa; 2) 100, 30.07, 150; 3) 100, 21.16, 225; 4) 70, 20.25, 150; 5) 70, 30.41, 150, 6) 70, 20.67, 232; 7) 70, 26.4, 232. Points from experiment, lines from numerical simulation; liquid: glycerol dissolved in distilled water. v_ℓ in m/sec and z in mm.

1) calculating droplet diameter:

$$d_d = \sqrt[3]{1{,}5\, d_n \lambda_{d^0}},$$

2) determining the effective density:

$$\bar{\rho} = \frac{\rho_g}{\rho_\ell}\left(\frac{d_d}{d_n}\right)^2,$$

3) calculating the Reynolds number:

$$\mathrm{Re} = \frac{v_{d0} d_d}{\nu_g},$$

4) determining the dimensionless coordinate at the end of the path:

$$\bar{z}_{de} = \frac{8}{\mathrm{Re}} \frac{z_{de}}{d_d},$$

5) determining the relative retardation from Fig. 2 and deriving the speed at the end of the path.

The set of experiments covered an extensive range (in the experiment sequence):

$$d_d \in \{208;\ 181{,}4;\ 222;\ 159;\ 137;\ 170;\ 158\},\ \mu\mathrm{m},$$
$$\mathrm{Re} \in \{190{,}5;\ 145{,}4;\ 227{,}95;\ 118{,}2;\ 97{,}83;\ 158{,}7;\ 149{,}52\}.$$

The relative errors in the numerical calculations on the velocity (by comparison with experiment) were

$$\Delta \in \{0{,}5;\ 2{,}6;\ 1{,}9;\ 1{,}2;\ 2;\ 2{,}9;\ 1{,}1\},\ \%.$$

This model predicts the retardation of a regular chain with high accuracy. The lateral retardation is almost linear. The retardation throughout the path is from 3 to 8% in relation to the initial velocity. The agreement between theory and experiment implies that for distances between droplets of about 1-4 d_d, the axial pressure gradient is $\partial p/\partial z = 0$, i.e., the air between the droplets forms a jet and is transported along with the droplets (compressor without piston and friction). This limiting case enables one to examine the effect of lateral retardation in pure form. As λ/d_n increases, the radial activity of the air between the droplets increases and one gets an axial gradient $\partial p/\partial z > 0$. This experimental method and system differ from those in Lee's method in enabling one to vary the distances between dropets almost without limit, i.e., they enable one to examine a continuous jet, a chain, and the intermediate range. The other limiting case is where the droplets are isolated and frontal resistance predominates. The method thus enables one to examine the jet, chain, and single droplet cases.

The model also enables one to derive the boundary-layer geometry and velocity profile throughout the path for undeflected and deflected chains. The trapped (undeflected) or deflected chain (or group) moves in an expanding fashion away from the end of the nozzle, with an associated air jet, and with a logarithmic velocity profile that varies along the path. The method developed for deriving the boundary-layer geometry enables one to detect wall effects and to eliminate adverse consequences from them in the design of printing heads, as they can adversely affect the focussing and the printing quality. Otherwise, one can proceed as follows. Symmetrical or unsymmetrical retardation and path curvature can occur in the charging electrode, the effects being related by

$$F = \eta \frac{S dv}{dy} \tag{15}$$

and increasing as h_3 decreases and ℓ_3 increases, and also as the area covered by the jet increases. To reduce the defocussing, retardation, and curvature, one should reduce ℓ_3 and adjust the system to eliminate the asymmetry. The condition for eliminating those shortcomings completely is

$$h_3 \geqslant d_d + 2\delta(z). \tag{16}$$

For the same purposes, the internal profile of the inductor can be adjusted to coincide with the external profile of the boundary layer (not in contact), which is also true for other electrodes and walls (the condition for excluding the wall effect).

A wall effect can occur that increases along the path on account of being near a plate in the deflecting system if the jet enters unsymmetrically, which retards the jet and draws it over to the plate, even to contact. There will also be an additional spread in the paths. To eliminate these effects, one needs to determine the inner profile for the deflecting plates from the outer profile of the boundary layers for the two limiting droplet chains (uncharged and charged or bipolar charged). A difference from existing designs is that the forbidden zone will expand along the paths. The condition for excluding the wall effects in the deflecting system (constraint for the upper edge of the letters) is

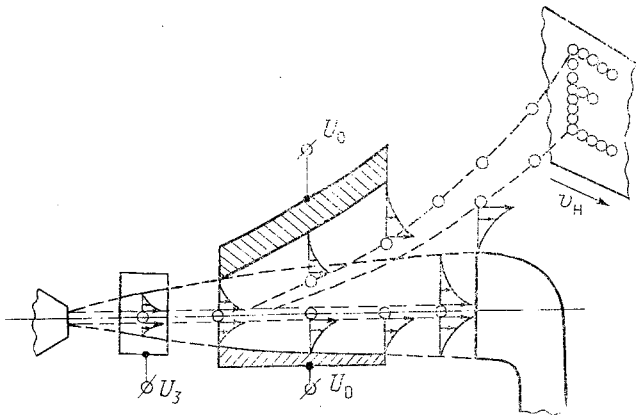

Fig. 6. Scheme for printing head illustrating the effects of the boundary layer and the wall on droplet chain flight.

$$h_3(z) \geqslant d_d + S(z) + 2\delta(z). \tag{17}$$

These results enable one to optimize the various types of deflecting electrode: plane-parallel with inclination relative to the path, rectilinear with oblique setting, and with second-order profile and so on. The optimization from the boundary-layer and wall-effect viewpoint (accuracy and printing quality) should be accompanied by optimization on deflection performance (minimizing the dimensions and the deflecting voltage).

The most extensive associated air jet occurs in the zone of the trap for the unused droplets. To eliminate vorticity in the trap, the dimensions and design should provide for taking up the entire flow of transporting air, i.e., it should overlap the entire boundary layer or deflect it away from the working paths. The wall effect for low paths for charged droplets will cause a spread in the lower points in the printing. To eliminate interaction between the boundary layers for the trap chain and the lower paths, it is necessary to meet a condition for the first path in the trap zone (constraint on the lower printing edge):

$$S_1(z) \geqslant 2\delta(z) + d_d. \tag{18}$$

In order to eliminate the effects from the boundary layer in the trap chain as far as possible, the trap should be placed as close as possible to the nozzle, e.g., be combined with the charging or deflecting electrode, and in the limit, it may be placed directly at the exit from the deflecting system. For that purpose, the trap chain can be charged with the opposite polarity and deflected sharply to the opposite side from the working paths (one can use a special slot in the deflecting plate). This is particularly important in binary drop control: yes to paper and no to trap.

Elevated resolving power is required for a multijet printing head, i.e., reduced step t between the centers of the nozzles, which tends to conflict with the requirement for raising the printing quality, since the boundary layers begin to interact. It is therefore necessary to meet the constraint

$$t \geqslant d_d + 2\delta(z). \tag{19}$$

Theory and experiment show that there is a difference from electrostatic interaction between droplets in a chain, which leads to defocussing in a jet (after initial perturbation), in that a boundary layer tends to produce self-focussing (at traction) and self-ordering. This applies for the y coordinate, while the converse applies for the z one (the Coulomb force produces repulsion, while the aerodynamic one produces convergence). The boundary layers and the wall effects in the main curve the paths, while the frontal resistance retards the drops and brings them together.

Boundary-layer calculations can be made from this model for an uncharged trap chain and with some approximation for a charged one, and also for ordered groups and even single droplets. It is true that a deflected chain, a group, or a single droplet will show increased effects not only from the side retardation but also the frontal. If the retardation is 3-5%

in an undeflected chain, it may attain 10% in a deflected one, which is due to the additional frontal resistance and also to each successive drop entering the peripheral boundary layer from the preceding one. The lateral retardation in a chain is 3-10%, while the frontal retardation for a single drop is 35-40%. In particular, in one of the experiments (No. 4), we found F_f = 1.5 μN and F_ℓ = 0.4 μN. The boundary-layer thickness (Fig. 6) in the electrode zone was $1.5d_d$ (238 μm), as against $2.5d_d$ (400 μm) on entry to the deflecting field, $4.5d_d$ on exit (715 μm), and $6d_d$ (954 μm) at the trap (substrate). This model and these constraints represent part of a general model for controlled flight, and they provide a basis for designing printing heads. Some of the processes have been simplifed, and in particular, the Magnus effect has been neglected when working drops leave the boundary layer, i.e., drop spin and lift.

NOTATION

ρ_g, gas density; z, axial coordinate; y, radial coordinate; δ, boundary-layer thickness; v_g, gas speed; ρ_ℓ, effective density of liquid; a, effective jet radius; v_ℓ, droplet speed; ν_g, kinematic viscosity of gas; $v_{\ell 0}$, initial velocity of droplets; $\bar{z}$ and $\bar{\rho}$, dimensionless coordinate and density; Re, Reynolds number; d_n, nozzle diameter; d_d, droplet diameter; f_d, droplet formation frequency; λ_d, distance between drops; z_{de}, coordinate for end of drop path; $\bar{z}_{de}$, dimensionless coordinate at end; Δ, relative calculation error; p, pressure; F, resistance; η, dynamic gas viscosity; h_3, inductor height; ℓ_3, inductor length; S, droplet cross section; t, step in multijet head; F_f, frontal resistance; F_ℓ, lateral force.

LITERATURE CITED

1. H. C. Lee, IBM J. Res. Develop., No. 1, 48-51 (1977).